Postharvest Biology and Technology 86 (2013) 249–258

Contents lists available at ScienceDirect

Postharvest Biology and Technology

journal homepage: www.elsevier.com/locate/postharvbio

# Supervised classification of bruised apples with respect to the time after bruising on the basis of hyperspectral imaging data

Piotr Baranowski*, Wojciech Mazurek, Joanna Pastuszka-Woźniak

*Institute of Agrophysics, Polish Academy of Sciences, ul. Doswiadczalna 4, 20-290 Lublin, Poland*

ARTICLE INFO

*Article history:*
Received 22 February 2013
Accepted 6 July 2013

*Keywords:*
Apple bruising
Time after bruising
Hyperspectral imaging
Supervised classification

ABSTRACT

Apple bruising, as a mechanical damage, occurs due to impact, compression, vibration or abrasion during handling. However, the symptoms of this damage, browning and softening of the tissue, appear not immediately but after a certain period of time after bruising. For sorting and grading systems, the information about how long the bruise exists in affected fruit can be valuable. VNIR (visible and near-infrared) and SWIR (short wavelength infrared) spectral characteristics of sound and bruised apple tissues were analyzed during a two week period after bruising. Supervised classification methods, including support vector machines, linear logistic regression, neural networks and decision trees, were used and compared to check their effectiveness for distinguishing time after bruising with respect to five varieties of apples. The detection system included hyperspectral cameras equipped with sensors working in the visible and near-infrared (400–1000 nm) and short wavelength infrared (1000–2500 nm) ranges. The results of supervised classification revealed good applicability of hyperspectral imaging in VNIR and SWIR spectral ranges for detecting the number of days after bruising. The linear logistic regression neural networks models were found to be the best classifiers in the majority of models developed. Prediction accuracies higher than 90% were obtained for classification models on spectral data pretreated with the second derivative.



## 1. Introduction

Bruise damage can be caused in apples from impact, compression, vibration, or abrasion (Leemans et al., 2002; Brosnan and Sun, 2004; Sun, 2008, 2010). In addition, the susceptibility of apples to bruise damage depends on the mechanical properties of the skin and flesh, which are cultivar dependent and can be modified by soil cultivation, nutrition and weather conditions in the field during fruit growth (Ferguson et al., 1999; Xing et al., 2007; Drogoudi and Pantelidis, 2011; Lleó et al., 2011; Grimm et al., 2012). Therefore, the location, shape and depth of bruising vary and damage detection is difficult, especially in case of dark skin colour or a small surface area of the bruise (Sun, 2008). Although bruising is the reason for rejecting the most fruit in sorting lines, the accuracy of the existing automatic sorting systems is still insufficient and a manual sorting method has still to be used (Leemans et al., 2002; Qin et al., 2009).

It is especially difficult to distinguish fruit bruises in the first hours/days after damage occurrence (Upchurch et al., 1994; Xing et al., 2005). Two basic effects of apple bruising, i.e. browning and softening of fruit tissue, develop gradually, depending on the storage conditions and physico-chemical properties of affected apples. The application of optical imaging in the visible and NIR regions for detection of early bruises is difficult due to multicolour backgrounds of particular cultivars (Wen and Tao, 2000; Xing et al., 2005). However, combining various wavelengths in differential reflectance improves detection and often identification of defects (Kleynen et al., 2003; Chen and Kim, 2004; Peng and Lu, 2006; Lee et al., 2008; Mendoza et al., 2011; Wang et al., 2011), and predicting fruit physical properties and biological variability (Lu, 2004; Lu and Peng, 2006; Nicolai et al., 2007; Peng and Lu, 2008; Bobelyn et al., 2010). A multispectral system was created (Mehl et al., 2002) which used the chlorophyll absorption wavelength at 685 nm and two wavelengths in the NIR range to separate defective areas in four cultivars of apples, with high spatial resolution between 0.5 mm and 1 mm. X-ray imaging was also tested for early apple bruise detection (Schatzki et al., 1997). However, the line-scan X-ray imaging experiment revealed inadequate separation of one day bruises in 'Golden Delicious' and 'Red Delicious' fruit (Shahin et al., 2002).

Baranowski et al. (2009) applied active thermal imaging for detection of early bruises in apples. The research was based on an hypothesis that internal defects and physiological disorders of fruit lead to changes inf tissue thermal properties. A comparison of pulsed-phase thermography (PPT) and visual inspection of bruising was performed, indicating high possibilities of the active thermography method for detecting defects up to several millimetres.

* Corresponding author. Tel.: +48 81 7445061; fax: +48 81 7445067.
*E-mail address:* pbaranow@ipan.lublin.pl (P. Baranowski).

0925-5214/$ – see front matter © 2013 Elsevier B.V. All rights reserved.
http://dx.doi.org/10.1016/j.postharvbio.2013.07.005

There is an increasing number of studies examining fruit quality, including bruises, using hyperspectral imaging (Lu et al., 1999; Kim et al., 2001; Lu, 2003; Mehl et al., 2004; ElMasry et al., 2009; Huang and Lu, 2010). The potential of a hyperspectral imaging system working in the spectral region from 400 nm to 1000 nm was studied for early detection (<12 h) of bruises in 'McIntosh' apples (ElMasry et al., 2008; Sun, 2010). This system allowed detection of apple bruises on different background colours (green, red, and green-reddish). High separation ability was reached for apples presenting recent (1 h) and old (more than 3 days) bruises. Hyperspectral imaging was useful for detecting bruising by applying the principal component (PC) transform and minimum noise fraction transform (MNF) methods (Lu, 2007). The multiplication of the first and third PC images, which were acquired by applying the PC transform to all pixels of the hyperspectral images along the spectral axis, gave images in which the bruised areas were repeatedly darker than normal tissue. The author noticed that the bruised regions were visible in the third MNF images and that the difference in reflectance between normal and bruised apples was greatest between 900 nm and 1400 nm.

The application of supervised classification methods becomes effective in distinguishing early and old damage of apple tissues. The backpropagation neural networks (BPNN), the decision tree, the *K*-nearest neighbour and a Bayesian classifier were used by Kavdir and Guyer (2004) to distinguish surface quality conditions of 'Empire' and 'Golden Delicious' apples. The classification accuracy using textural features ranged between 72.2% and 100% for 'Empire' apples and between 76.5% and 100% for 'Golden Delicious' apples. A systematic approach was developed using hyperspectral imaging in conjunction with partial least squares regression (PLS) as well as stepwise discrimination analysis to define several optimal wavelengths in hyperspectral analysis of apples (ElMasry et al., 2009). The artificial neural networks were also used by ElMasry et al. (2008) to select the optimal wavelengths, to classify the apples, and to detect firmness changes due to chilling injury. Baranowski et al. (2012) created a system that included hyperspectral cameras equipped with sensors working in the visible and near-infrared (400–1000 nm), short wavelength infrared (1000–2500 nm) and thermal imaging camera in mid-wavelength infrared (3500–5000 nm) ranges. The comparison of the results obtained using the supervised classification methods, including Soft Independent Modelling of Class Analogy (SIMCA), Linear Discriminant Analysis (LDA), and Support Vector Machines (SVM), confirmed that the broad spectrum range (400–5000 nm) of fruit surface imaging can improve the detection of early bruises with varying depths. From a practical point of view, a potential possibility to evaluate how long the bruise defect maintains would give a chance to sort and grade the apples more effectively. This information would enable better prediction of susceptibility of affected apples to infections. Therefore, the aim of this study was to examine the applicability of hyperspectral imaging in VNIR and SWIR wavelength ranges for classification of apple bruising with respect to the time after damage of five selected cultivars.

## 2. Materials and methods

### 2.1. Material and its preparation for measurements

Apples were collected from an orchard of the 'STRYJNO-SAD' Fruit Producers Association (15 km from Lublin, Poland), directly after hand harvesting in autumn 2011 and 2012. Five apple (*Malus domestica* Borkh) cultivars, 'Champion', 'Gloster', 'Golden Delicious', 'Idared' and 'Topaz', were selected for the study to create diverse material according to colour and physico-chemical properties. During hyperspectral measurements, which lasted for two weeks, the apples were stored in a climate chamber at 3 °C and 80% RH, and removed to the laboratory conditions (21 °C) only for measurements. Apples with a diameter of 7–8 cm of each cultivar were selected for analytical analysis and hyperspectral measurements.

Bruised and unbruised regions were studied with an hyperspectral system using a total of 580 apples (480 of which were used as a training set for supervised classification and 100 as a testing set). Each apple was bruised along the equatorial line of its surface. A plastic cylinder with a diameter of 10 mm and a thickness of 1 mm was used for bruising. It was applied vertically on the apple surface (the apple was lying with its equatorial area touching the table surface) and a cylindrical weight of 0.2 kg was dropped (the contact surface was the base of the cylinder) from a height of 400 mm (Baranowski et al., 2012).

### 2.2. Analytical measurements

At the beginning and end of the experiment, measurements of basic physical properties of the apples were done. Fruit firmness was measured using a Lloyd LRX Universal Testing Machine, produced by Lloyd Instruments Ltd., Hampshire, UK, equipped with a cylindrical tip of 11.3 mm in diameter made of steel. A tip was moving at a constant speed of 8 mm/s towards the fruit with skin slice removed. The firmness was taken as the maximum force needed for the tip to penetrate the fruit to a depth of 8 mm. Three measurements of firmness were made on each fruit, in the pedicle area, the middle part of the apple, and in the calyx area. The means of these three firmness readings were expressed in *N*.

Soluble solids contents (SSC) were determined using an Atago pocket refractometer produced by Atago Co., Ltd., Tokyo, Japan, at ambient temperature of 20 °C. For each apple, two measurements of SSC were made at the opposite sides of the fruit, with three replications for each side. The averaged values of these measurements were analyzed. The values obtained were expressed in %.

Apparent densities of apples of all studied cultivars were determined. Each apple was weighed with an electronic digital Mettler XS1003S balance, Mettler Inc., Switzerland (operating capacity of up to 1000 g with a readability of 0.001 g), and apple volumes were determined through the measurement of the water volume displaced by the fruit.

### 2.3. Hyperspectral imaging system

Hyperspectral imaging systems enable complex information on the studied objects to be obtained. A hyperspectral image consists of spatial (2-dimensional) and spectral (1-dimensional) data. They create a 3-dimensional spectral cube in which the spectral characteristics of selected pixels can be studied, while images obtained for various wavelengths can be analyzed with the use of available image processing methods.

In this study, two linear hyperspectral scanners were used as the hyperspectral system: a visible and near infrared (VNIR) camera with an ImSpector V10E imaging spectrograph (400–1000 nm) and a short wavelength infrared (SWIR) camera with a N25E 2/3″ imaging spectrometer (1000–2500 nm) manufactured by SPECIM, Finland. The set up of this system is presented in Fig. 1. The cameras were mounted 40 cm above a belt conveyor which had the speed regulated for each camera (to perform line scanning of the fruit). The illumination source in the system consisted of 12 halogen lamps of 20 W each placed in the inside bottom part of a hemispherical diffuser. The lamps were placed along the perimeter at the angular distance of 30°. The lamps illuminated the diffuser inner surface made of aluminium. The diameter of the diffuser's dome was 50 cm. The diffuser allowed homogeneous illumination of the scanned surface of the apple to be obtained. The lamps were powered by three 12 V DC power supplies. The measurements were

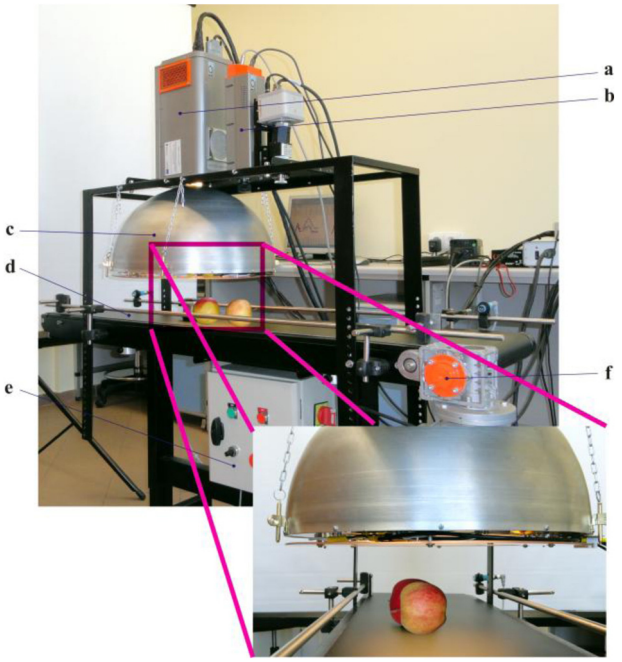


**Fig. 1.** Setup for hyperspectral measurements consisting of: (a) SWIR spectral camera; (b) VNIR spectral camera; (c) diffuser with halogen lamps; (d) belt conveyor with photocells for controlling the direction of movement; (e) system for regulation of belt conveyor speed; (f) stepper motor.

performed in a dark room to prevent the influence of external illumination. For each camera, speed of the belt conveyor movement during line scanning was adjusted individually to suit differences in spatial resolution and integration time of the cameras. The average speed of the belt conveyor was 0.025 m/s. The resolution of the VNIR camera image was 1344 (spatial) by 1024 (spectral) pixels by 12 bits, which corresponds to a root mean square (rms) spot radius of less than 40 μm and a spectral resolution of 6.8 nm (with 30 μm slit width). The lens with focal length of 23 mm, *F*-number 2.4 and maximum spatial image size of 14.4 mm was used with the VNIR camera.

The image from the SWIR camera had a resolution of 320 (spatial) by 256 (spectral) pixels by 14 bits, which corresponded to an rms spot radius of less than 15 μm and a spectral resolution of 10 nm (30 μm slit). The lens with focal length of 30.7 mm, *F*-number 2.0 and maximum spatial image size of 12.8 mm was used with the SWIR camera. The exposure time for the VNIR camera was about 3.6 ms and for the SWIR camera it was about 7.2 ms. The lenses of VNIR and SWIR cameras were equipped with spectral flattening filters: SP-SFVNIR/40 and SP-SFSWIR/40 by SPECIM, Finland, respectively.

The hyperspectral images from the two cameras were recorded on a PC computer using data acquisition software SpectralDAQ ver. 2.1 for SPECIM cameras. The acquisition time of one scan of the fruit surface for the VNIR and SWIR cameras was 5 s.

For each series of measurements, white and dark calibrations were done to obtain the reflectance *R* from the raw data according to the following formula (Sun, 2010):

$$R = \frac{I_{im} - I_{bl}}{I_{wh} - I_{bl}} \quad (1)$$

where $I_{im}$ is the intensity of an image; $I_{wh}$ is the intensity of the white reference Spectralon plate with a reflectance of 99% (R99), Labsphere Inc., North Sutton, NH, USA; and $I_{bl}$ is the intensity of the dark image (the shutter closed, the light sources turned off and the lens covered with a black cap).

### 2.4. Analyzing algorithms

For each sample, the areas containing bruised or non-bruised regions were selected from the hyperspectral cube. To distinguish the areas of bruising, a script was written using ImageJ software (Rasband, 1997–2011). The segmentation scheme is presented in Fig. 2, which is a modification of the procedure proposed earlier by ElMasry et al. (2009). From the hyperspectral cube of a studied apple, one image was selected to create the binary mask of the fruit (it was in majority of cases the 540 nm image). Other 41 images at wavelengths from 680 nm to 960 nm were averaged to create the binary mask of the bruised area. The binary mask of the fruit surface was put on the averaged image of these wavelengths to eliminate the background. The implementation of the Otsu thresholding algorithm was used to distinguish the bruised area. It divides the histogram into two classes and the inter-class variance is minimized. Additionally, particle nucleus counting was applied to this image which allowed regions of sizes ranging from 50 to 5000 pixels to be distinguished. The average reflectivity from all the pixels in these regions (containing bruised and sound tissues) was calculated for all the bands separately. The averaged spectral characteristics of bruised and sound areas of all studied apples were gathered in an Excel 2007 database which was then transposed into ARFF format (native file format in Weka).

The pretreatment of spectral characteristics was completed with the use of The Unscrambler® X ver. 10.1, CAMO Software, Oslo, Norway. The classification results for the data pretreated with various methods were compared. The following pretreatment methods were applied to obtained spectral characteristics of bruised and unbruised areas of the apple samples: baseline offset with linear baseline correction (BOL), multiplicative scatter correction (MSC), standard normal variate with detrending (SNV&DT) and second derivative calculated with Savitzky–Golay method (fourth polynomial order and 11 smoothing points). The baseline correction is used to adjust the spectral offset by either adjusting the data to the minimum point in the data (baseline offset), or by making a linear correction based on two user-defined variables (linear baseline correction. In this study these two transformations were executed together. The multiplicative scatter correction (MSC) is used to compensate for additive and/or multiplicative effects in spectral data. It consists of fitting a separate regression line to each sample spectrum, expressed as a function of the average value for each wavelength; the coefficients of that regression line are then used to correct the values of each sample. The result of SNV is that it removes scatter effects from spectral data. The detrending (DT) is a transformation which helps to remove non-linear trends in spectroscopic data. Finally, standard normal variate in combination (SNV&DT) are applied to reduce multi-collinearity, baseline shift and curvature. The second derivative is a measure of the change in the slope of the curve. In addition to ignoring the offset, it is not affected by any linear "tilt" that may exist in the data, and is therefore a very effective method for removing both the baseline offset and slope from a spectrum.

Pre-processing of the hyperspectral data consisted in choosing, from the whole spectral range registered by the two cameras, the range in which the spectral characteristics of the signal were sufficiently strong. To avoid the low signal–noise ratio, only the wavelengths ranging from 432 nm to 2450 nm were used for classification with approximately 6 nm increments per pixel. In this way, 344 channels represented independent variables in the created models.

The problem of high dimensionality of feature spaces, known as Hughes phenomenon or curse of dimensionality has been considered in this study by applying the Correlation based Feature Selection algorithm (CFS) to the original spectral data (Hall, 1998). It evaluates the worth of a subset of attributes by considering the

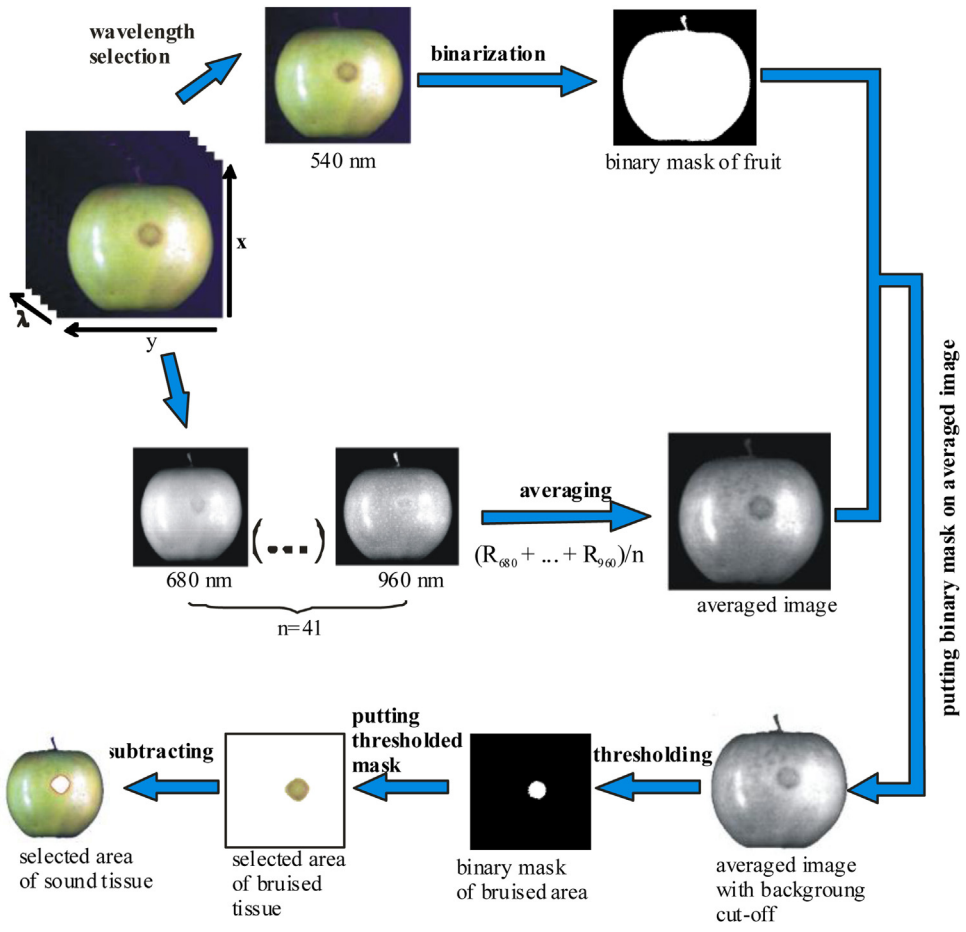


**Fig. 2.** Procedure for hyperspectral image segmentation.

individual predictive ability of each feature along with the degree of redundancy between them. The best-first search method was applied in this algorithm with forward direction.

The classification experiments were performed on the hyperspectral data of the fruit surface (selected randomly 480 instances for the training set and 100 instances for the testing set). The experiment of learning and testing was repeated 10 times with random data selection (cross validation method). For each fold, the proportion between the data used for learning and data used for testing was 90–10%. It has been confirmed (Witten and Frank, 2005) that the stratified 10-fold cross-validation is a standard evaluation technique in situations where only limited data is available and it is regarded as the most rigorous one. The idea of 10-fold cross validation is that data are partitioned randomly into 10 complementary subsets. Each subset is held out in turn and the learning scheme trained on the remaining nine-tenths. Then, its error rate is calculated on the holdout set. The learning procedure is executed a total of 10 times on different training sets.

All classification algorithms were implemented from the Waikato Environment for Knowledge Analysis software, called "Weka" (Witten and Frank, 2005).

In this study, two categories of "Weka" classifiers were used: functions and trees. Initially, the majority of available classifiers in these categories were tested on representative groups of training and testing data. Eight of them with best prediction accuracies were chosen for comparison. These classifiers are presented in Table 1, together with a general description and the actual parameters determined in this study.

Weka Knowledge Flow Interface was used for all the studied classifiers in which dependent variables in classification models were six periods after bruising (2nd day, 5th day, 6th day, 9th day, 12th day, and 14th day). This graphical interface allows the design and execution of configurations for streamed data processing.

## 3. Results

### 3.1. Physical properties of studied cultivars

During the storage of the fruit in the climatic chamber for 14 days, the measured physical properties of the fruit did not change significantly. Therefore, it was decided to average the measured values from the beginning and the end of experiment for apples of individual cultivars. The averaged values ($N = 30$) of firmness, soluble solids content and density of the fruit with standard error bars are presented in Fig. 3. The highest mean values of firmness (52.1 N and 43.4 N) and density (1090 kg/m$^3$ and 980 kg/m$^3$) as well as the lowest mean values of soluble solids content (12.4% and 13.6%) were noted for the cultivars 'Idared' and 'Topaz', respectively. It was expected that the differences in these properties between cultivars affected the spectral characteristics of apples.

### 3.2. Reflectance spectra

An exemplary reflectance spectra on successive measurements days obtained for 'Golden Delicious' apples in the VNIR and SWIR ranges are presented in Fig. 4 for sound and bruised tissues,

**Table 1**
Chosen features of the classifiers used in the study.

| Type of classifier | Name of classifier's library | Description of algorithm | Acronym | Chosen parameters of classifier |
|---|---|---|---|---|
| Functions | SMO | Sequential minimal optimization algorithm for support vector classification | SMO | Filter type: normalize; training data; Kernel: PolyKernel C-250007-E1.0 |
| | Simple logistic | Builds linear logistic regression models with built-in attribute selection | SL | Heuristic stop: 50; MaxBoostingIterations: 500; NumboostingIterations: 0 |
| | Logistic | Builds linear logistic regression models | LLR | Debug: false; MaxIts: −1; Ridge: 1.0E-8 |
| | LibSVM | A wrapper class for the libsvm tools. Runs faster than SMO. Allows users to experiment with One-class SVM, Regressing SVM, and nu-SVM supported by LibSVM tool | SVM | SVM Type: nu-SVC; Kernel Type: radial basis function; Nu: 0.5; Normalize: true |
| | LibLINEAR | A wrapper class for the liblinear classifier | LINE | SVM Type: L2 loss support vector machines; Bias: 1.0; Normalize: true |
| | Multilayer perceptron | Uses backpropagation neural networks to classify instances | BNN | AutoBuild: true; Learning rate: 0.3; Momentum: 0.2; Training time: 500 Hidden layers = (attribs + classes)/2 |
| Trees | FT | Classifier for building 'Functional trees', which are classification trees that could have logistic regression functions at the inner nodes and/or leaves | FT | BinSplit: false; Model type: FT; NumBoostingIterations: 15 |
| | LMT | Classifier for building 'logistic model trees', which are classification trees with logistic regression functions at the leaves | LMT | Fast regression: true; MinNumberInstances: 15; NumBoostingIterations: −1 |

respectively. In this figure, the spectra were obtained from ROIs distinguished using the procedure presented in Fig. 2, which represented the average for sound tissues (on the left in the figure) as well as bruised tissue (on the right). Apart from the raw spectral characteristics on the succeeding measurement days (first row in Fig. 4), particular pretreatment transformations of the spectral characteristics are presented, including the baseline offset with linear correction (BOL), the multiple scatter correction (MSC), the standard normal variate in combination with detrending (SNV&DT) and second derivative. In all the spectral characteristics the typical water absorption bands, i.e. 660 nm, 970 nm, 1200 nm, 1470 nm and 1900 nm appear as localized minima. The carotenoids and chlorophyll pigments are reflected through the absorption valleys around 500 and 680 nm (ElMasry et al., 2008). The courses of spectral characteristics for 'Golden Delicious' and their transformations, presented in Fig. 4, are typical for all the studied varieties. It reveals the considerable changes in reflectance from bruised tissues, in particular, days after bruising, especially in the spectral range from 900 nm to 1900 nm, as compared to the sound tissue. The differences in reflectance between succeeding measurement days were also observed in the range from 750 nm to 850 nm for bruised tissue. However, similar changes in this spectral region were observed for sound tissue (raw spectral data and baseline offset with linear correction). In this spectral region (750–850 nm) application of MSC and SNV&DT transformations enabled much higher differentiation of spectral characteristics between particular days after bruising for bruised tissue than for sound tissue. In the visible spectral range from 400 nm to 780 nm, changes of spectral characteristics during the measurement days were smaller, both for bruised and sound tissues. However, in this range, the differences in spectral characteristics between bruised and sound regions are meaningful, as is clearly seen in the last row of Fig. 4, representing the second derivative transformation.

### 3.3. Supervised classification models

The supervised classification models were created to distinguish between days after bruising for apples of all five cultivars for the eight classifiers tested (their parameters described in Table 1). The class of days after bruising consisted of six elements (2nd, 5th, 6th, 9th, 12th, and 14th days). The general information on prediction accuracy of the created models is presented in Fig. 5 (the first row in the table below the plot presents the results for original data). In this group of models, the best prediction accuracy was observed for the linear logistic regression model (LLR) – correctly classified instances (97.7%). Two other models with the highest number of correctly classified instances were as follows: the logistic model trees (LMT) – 94.5%, and the backpropagation neural networks (BNN) – 89.9%. The other classification models had considerably lower prediction accuracies with the percentage of correctly classified instances between 68.7% and 86.6%.

To illustrate how the cases belonging to different classes were classified by the particular models, the confusion matrices were created. An example of a confusion matrix for the linear logistic regression model (LLR) is presented in Fig. 7. The rows in this matrix represent the actual outputs, while the columns the targets. The upper number in each entry of the matrix is the average number of the actually recognized classes in testing mode and the bottom one, its percentage, referred to the total number of all cases used in testing (480). The diagonal entries of the matrix represent the mean quantity of the properly recognized cases (the upper value) and also its ratio with respect to the total representation of all testing data (the lower value is expressed as a percentage). Each entry outside the diagonal means an error (the number of misclassifications and its relative value). It is seen that the highest number of misclassifications occurred for the 2nd day (4 cases) and for the 5th day (4 cases) after bruising. The last column of the matrix represents the total percentage measure of accuracy of actual recognition for the class pointed by the classifier. Again, it can be read that the 2nd and 5th days after bruising have a lower total percentage measure of accuracy of actual recognition than the other classes. The upper number in this column represents the ratio of the number of the properly recognized cases to the total number of cases pointed by this particular output. The bottom numbers in the last column represent the false alarm ratios. The last row of the matrix represents the ratios of the number of the properly recognized cases to the total number of true cases (targets). The bottom numbers in this row are the misclassification ratios.

The results presented in Fig. 5 enabled comparison of the classification accuracies of eight studied classifiers for raw and transformed data. For all studied groups of reflectance data of days after bruising as the output class, a very high percent of correctly classified instances was obtained for linear logistic regression (LLR) classifier (higher than 97%). The best classification accuracies for

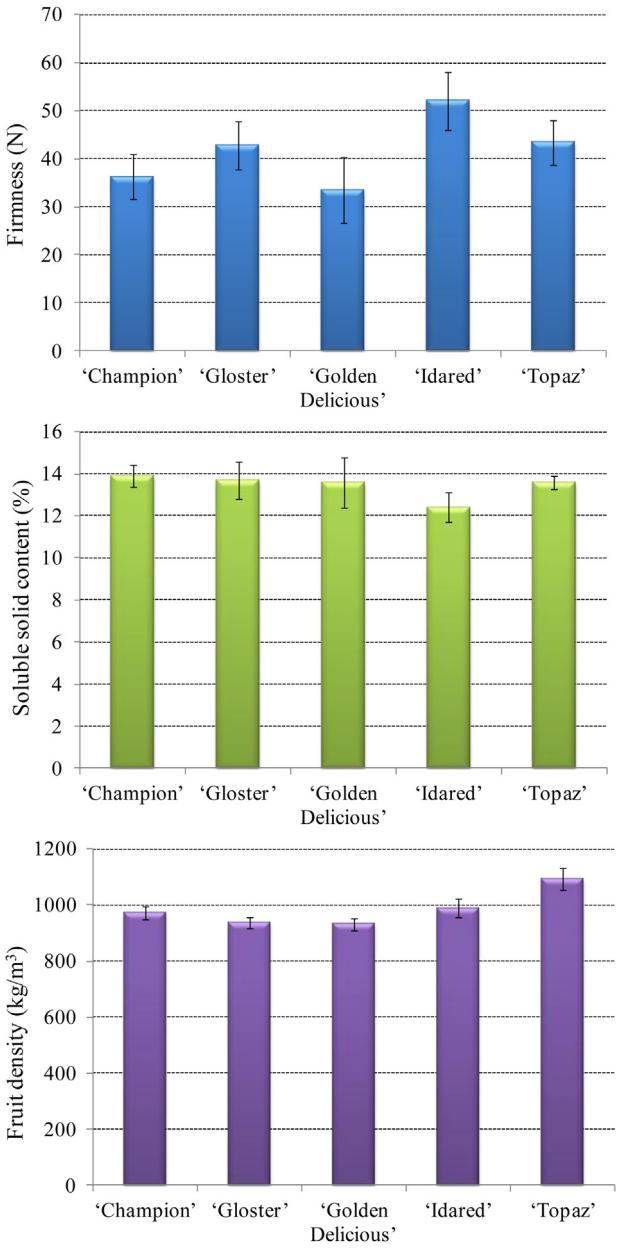


**Fig. 3.** Physical properties of the apple cultivars with indicated standard errors.

nearly all the classifiers were attained for the second derivative data with the highest accuracy of 99.4% in case of SMO classifier. The lowest prediction accuracy for majority of data groups was acquired for LibSVM (SVM) and LibLINEAR (LINE) classifiers.

The prediction efficiency of obtained models was checked on an independent test set consisting of 100 instances, chosen randomly from the whole data set. The results of the prediction accuracy of individual models of day after bruising as an output class are presented in Fig. 6. The highest percent of correctly classified instances was obtained for second derivative data by using the simple logistic (SL) model (95.4%). Five other classifiers gave more than 90% of correctly classified instances for the second derivative data. This result confirmed the usefulness of this derivative for discrimination of some hidden features of the spectra, mainly by removing overlapping peaks and at the same time correcting the baseline. For other groups of data (including raw data) the best prediction accuracies were gained by the use of neural networks (BNN) and logistic model trees (LMT) classifiers. For these classifiers prediction accuracies ranged from 89.0% to 91.6%. From among all the classifiers, the worst prediction power had the support vector machines (SVM) and Liblinear (LINE) classifiers with prediction accuracies not exceeding 80% for any data set.

### 3.4. Automatic attribute selection (CFS) and efficiency of models

In classification problems of hyperspectral data it is of great importance to be able to remove features of the data that are irrelevant or redundant with respect to the learning task. This process, called feature selection, was accomplished in this study by the use of fully automatic CFS (Correlation based Feature Selection) algorithm, which is based on the hypothesis that good feature sets contain features that are highly correlated with the class, but uncorrelated with each other. We wanted to know if the reduced feature sets would equal the accuracy using the complete feature sets of separate groups of data. The results of the feature selection procedure are presented in Table 2. The CFS algorithm considerably reduced the dimensionality of data needed to achieve learning. The number of selected bands ranged from 18 (original data after preprocessing) to 40 (second derivative). It looked alarmingly that from 18 selected bands of the original data, five were above 2400 nm (the ending of the spectral range in which signal was the weakest). On the other hand, the selected bands of the original, the MSC and the second derivative data started beyond 670 nm. In the majority of selected sets, water absorption bands were represented.

The selection algorithm reduced execution time of classification but did not worsen significantly the accuracy of the classification models. The results of classification for selected bands and days after bruising as output classes are presented in Fig. 8. Six classifiers for the second derivative set reached the prediction accuracies higher than 90%, similarly as in the case of the unreduced data set (comparable with Fig. 5). The limited number of selected bands (18) of raw data set considerably diminished the prediction accuracy of obtained models. Because second derivative pretreated wavebands, selected with the Correlation based Feature Selection algorithm gave the best prediction accuracies for majority of models, it was decided to use these 40 bands for comparing classification efficiency of linear logistic regression model in respect to separate cultivars. The results of this analysis are presented in Table 3. The highest percent of correctly classified cases was obtained for 'Golden Delicious' (97.9%) and 'Champion' (95.8%) cultivars. Two cultivars had significantly lower percents of correctly classified cases: 'Idared' (84.4%) and 'Topaz' (83.3%). It is seen from Fig. 3 that for these two cultivars, the averaged firmness and density values were the highest during the experiment and the soluble solids values were the lowest during the experiment. The highest number of misclassified bruises was noticed for the second and fifth days after bruise occurrence. On the last day of the experiment 100% classification accuracy was obtained for all cultivars.

## 4. Discussion

It has been confirmed in this study that hyperspectral imaging technology has good potential for detecting time after bruising effectively. The analysis of bruised regions in the apples studied revealed considerable changes in spectral characteristics in time (during two weeks after bruising with six measurements), especially in the spectral ranges from 750 nm to 850 nm and from 900 nm to 1900 nm. The reflectance of bruised regions changed significantly with the time after bruising for wavelengths characteristic for water absorption bonds, especially in 970 nm, 1200 nm, 1470 nm and 1900 nm. It confirms earlier reports that drying of

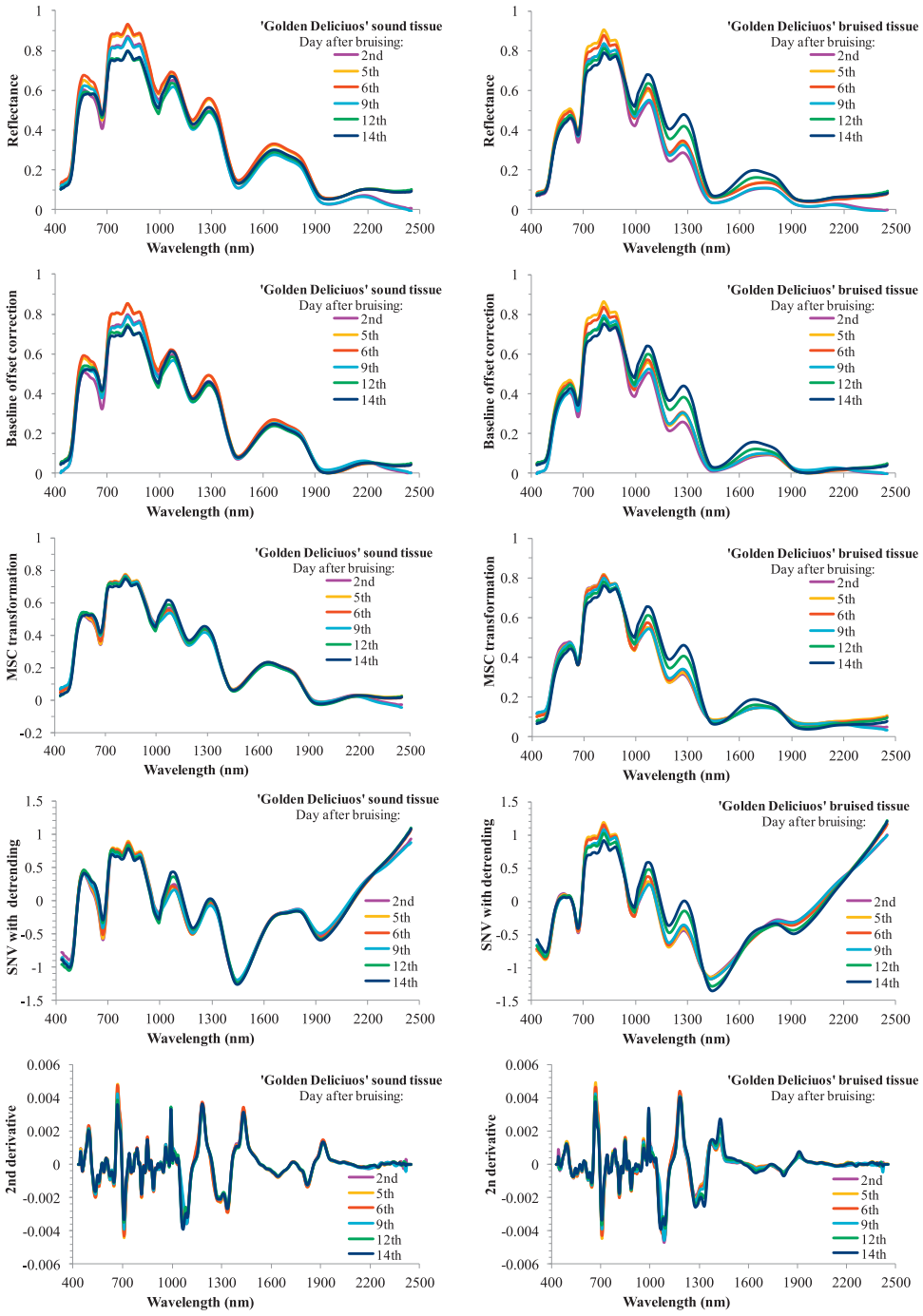


**Fig. 4.** Exemplary spectral characteristics and their preprocessing treatments of 'Golden Delicious' sound and bruised tissues on successive measurement days.

**Table 2**
The results of Correction based Feature Selection (CFS) procedure performed on original preprocessed data and transformed data. Selected bands were used in further supervised classification to distinguish days after bruising.

| Spectral data | Selected bands (Correlation based Feature Selection algorithm) | Number of selected bands |
|---|---|---|
| Original data after preprocessing | 760, 775, 817, 837, 969, 1017, 1074, 1093, 1188, 1200, 1219, 1263, 1270, 2426, 2432, 2438, 2444, 2450 | 18 |
| Baseline offset with linear baseline correction | 432, 437, 442, 447, 462, 477, 591, 713, 718, 734, 744, 749, 760, 801, 811, 822, 921, 1118, 1828, 1903, 1928, 1978, 2383, 2407, 2426, 2432, 2439, 2445, 2451 | 29 |
| MSC | 672, 718, 724, 729, 734, 749, 760, 780, 948, 953, 964, 969, 1017, 1024, 1030, 1036, 1125, 1200, 1226, 1377, 1433, 1446, 1471, 1483, 1496, 1546, 1552, 1559, 1903, 2165, 2289 | 31 |
| SNV&DT | 511, 561, 713, 948, 969, 1024, 1181, 1200, 1244, 1395, 1402, 1470, 1903, 2140, 2159, 2171, 2184, 2209, 2233, 2283, 2289 | 21 |
| 2nd derivative | 683, 713, 718, 744, 749, 760, 765, 770, 801, 806, 817, 827, 843, 879, 885, 948, 969, 1043, 1093, 1099, 1106, 1137, 1169, 1175, 1200, 1219, 1339, 1345, 1358, 1364, 1471, 1740, 1903, 2090, 2109, 2121, 2140, 2171, 2196, 2233 | 40 |

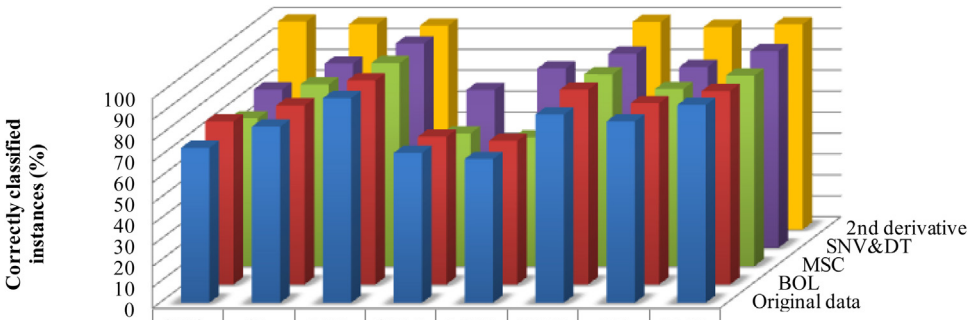


| | SMO | SL | LLR | SVM | LINE | BNN | FT | LMT |
|---|---|---|---|---|---|---|---|---|
| Original data | 74.0 | 84.1 | 97.7 | 71.6 | 68.7 | 89.9 | 86.6 | 94.5 |
| BOL | 77.9 | 85.5 | 97.4 | 70.6 | 68.6 | 93.0 | 86.6 | 92.4 |
| MSC | 70.6 | 86.8 | 97.0 | 63.4 | 61.5 | 91.6 | 84.6 | 91.0 |
| SNV&DT | 75.6 | 88.0 | 97.6 | 75.4 | 85.7 | 92.7 | 86.4 | 94.0 |
| 2nd derivative | 99.4 | 98.1 | 97.4 | 29.4 | 35.1 | 99.2 | 96.8 | 98.1 |

**Fig. 5.** Results of classification for distinguishing days after bruising for apples of all cultivars (models for original raw and transformed data). All 344 bands were included in model creation.

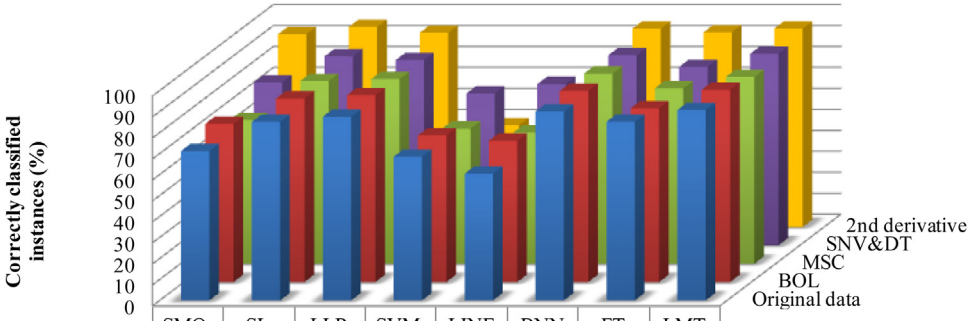


| | SMO | SL | LLR | SVM | LINE | BNN | FT | LMT |
|---|---|---|---|---|---|---|---|---|
| Original data | 71.2 | 85.1 | 87.5 | 68.5 | 60.4 | 90.0 | 85.1 | 90.7 |
| BOL | 75.4 | 87.5 | 89.1 | 69.9 | 67.4 | 91.1 | 82.8 | 91.6 |
| MSC | 68.4 | 87.1 | 88.0 | 64.4 | 62.5 | 90.6 | 83.6 | 89.0 |
| SNV&DT | 77.6 | 90.1 | 88.3 | 72.4 | 76.9 | 90.6 | 85.1 | 91.3 |
| 2nd derivative | 91.9 | 95.4 | 92.6 | 48.5 | 55.3 | 94.6 | 92.8 | 94.6 |

**Fig. 6.** Comparison of classification results on testing data set (100 instances) for classifiers and various data types (original and transformed data).


**Fig. 7.** The confusion matrix obtained with 10-fold cross validation for the linear logistic regression model.

the injured tissues influences spectral characteristics of the aged bruises (Upchurch et al., 1994).

The thorough comparison of several preprocessing procedures and classifiers, including five apple cultivars varying with basic physical properties, indicated second derivative transformation of the spectral data together with backpropagation neural networks and logistic regression classifiers as the most efficient for time after bruise classification. The best performance among the tested models for the class of days after bruising was noted for the following: the linear logistic regression (LLR) models, the logistic model tree (LMT), and the backpropagation neural networks (BNN).

The problem of evaluating how long the bruise exists in affected fruit is very important for apple grading systems, apple storage and shelf-life. However, this problem has not been studied thoroughly in previous studies on application of multi- and hyperspectral systems for detection of apple bruises. The majority of them have been concerned with the first hours after damage occurrence, usually one cultivar and limited numbers of classifiers applied (Upchurch et al., 1994; Xing et al., 2005). Affected apples are susceptible to infections and fungal diseases and knowing the time of bruise existence can improve apple storage and shelf-life handling. This information may not only be crucial for eliminating apples with bruise but also for estimating the possible harmful effects of the affected tissue on surrounding healthy apples. The novelty of the present study consists in application of very effective classification

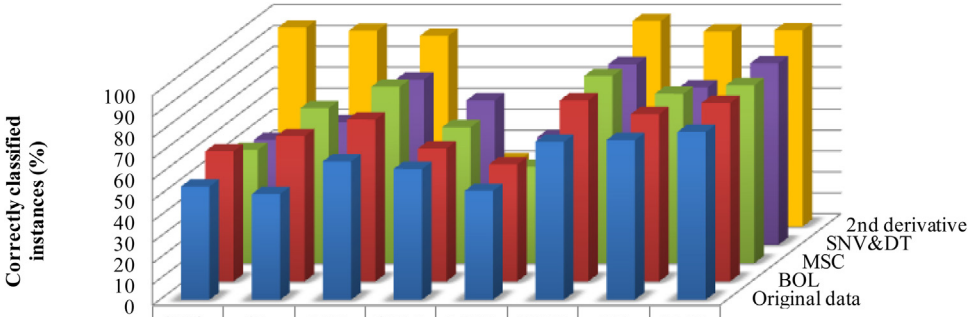


| | SMO | SL | LLR | SVM | LINE | BNN | FT | LMT |
|---|---|---|---|---|---|---|---|---|
| Original data | 54.1 | 50.5 | 66.1 | 62.5 | 52.0 | 75.5 | 76.3 | 80.2 |
| BOL | 62.2 | 69.4 | 77.3 | 63.5 | 55.9 | 86.5 | 79.9 | 85.3 |
| MSC | 54.1 | 74.0 | 84.2 | 64.9 | 46.0 | 89.4 | 80.9 | 85.0 |
| SNV&DT | 50.1 | 58.6 | 78.9 | 69.0 | 51.4 | 86.3 | 75.2 | 86.7 |
| 2nd derivative | 95.1 | 93.6 | 91.1 | 31.6 | 35.8 | 98.2 | 93.2 | 93.8 |

**Fig. 8.** Results of classification for days after bruising as output classes for the training set (480 instances) and bands selected with Correction based Feature Selection algorithm as inputs. Particular columns in this table represent results for selected bands of raw data and transformed data.

**Table 3**
Classification results of linear logistic regression model in respect to particular cultivars. Second derivative data (480 cases) was applied with 40 wavebands selected automatically with the use of Correction based Feature Selection algorithm.

| Cultivar | Correctly classified cases (%) | Misclassified cases (%) | | | | | |
|---|---|---|---|---|---|---|---|
| | | 2nd day | 5th day | 6th day | 9th day | 12th day | 14th day |
| Champion | 95.8 | 1.0 | 2.1 | 0.0 | 1.0 | 0.0 | 0.0 |
| Gloster | 93.8 | 3.1 | 1.0 | 1.0 | 1.0 | 0.0 | 0.0 |
| Golden delicious | 97.9 | 1.0 | 1.0 | 0.0 | 0.0 | 0.0 | 0.0 |
| Idared | 84.4 | 7.3 | 5.2 | 2.1 | 0.0 | 1.0 | 0.0 |
| Topaz | 83.3 | 8.3 | 3.1 | 2.1 | 2.1 | 1.0 | 0.0 |

procedures of classification and automatic selection of the most efficient wavelengths from the spectral data for evaluating time after bruising occurrence. The benefits of Correlation based Feature Selection (CFS) algorithm, are a considerable reduction in the amount of data needed to achieve learning model and a satisfactory predictive accuracy which was evident in the case of the input spectral data pretreated with second derivative (40 selected bands enabled to obtain prediction accuracy higher than 90%).

The results of our study show that the accuracy of the supervised classification with the use of the applied classifiers differs among cultivars and depends on physical properties of the apples, such as firmness, density and soluble solids content. It has been confirmed earlier that the speed, cost, and processing power of the available hyperspectral imaging systems make it more suitable for research than on-line applications (Lu, 2007; Sun, 2010). From this point of view, this study can be treated as a reference to help developing a multispectral imaging system in future for on-line determination of the time after bruising occurrence.

In conclusion, the results revealed good applicability of hyperspectral imaging in VNIR and SWIR regions for distinguishing time after bruise occurrence within the period of two weeks after bruising for the apples of five cultivars. Implementation of the elaborated algorithms of the supervised classification in existing sorting systems will require additional multisensory studies on interactions between physiological processes within affected tissues and their reflectance spectral characteristics. The respective sensors sensible for the spectral bands selected may be included into the sorting systems to permit defects to be distinguished with respect to the time of their occurrence. This information would improve the effectiveness of apple sorting and grading.

Possibilities of diminishing the size of spectral data by choosing the optimum method of attribute selection to shorten time of data acquisition and processing should be thoroughly tested on other cultivars. Improvements of the approach will also need to address the issues of physical and biochemical changes within affected tissues in time and necessity of creating fast multispectral sensors.

## References


Baranowski, P., Mazurek, W., Witkowska-Walczak, B., Slawiński, C., 2009. Detection of early apple bruise with the use of pulsed-phase thermography. Postharvest Biol. Technol. 53, 91–100.

Baranowski, P., Mazurek, W., Wozniak, J., Majewska, U., 2012. Detection of early bruises in apples using hyperspectral data and thermal imaging. J. Food Eng. 110, 345–355.

Bobelyn, E., Serban, A.-S., Nicu, M., Lammertyn, J., Nicolai, B.M., Saeys, W., 2010. Postharvest quality of apple predicted by NIR-spectroscopy: study of the effect of biological variability on spectra and model performance. Postharvest Biol. Technol. 55, 133–143.

Brosnan, T., Sun, D.W., 2004. Improving quality inspection of food products by computer vision – a review. J. Food Eng. 61, 3–16.

Chen, Y.R., Kim, M.S., 2004. Visible/NIR imaging spectroscopy for assessing quality and safety of agro-foods. In: Davies, A.M.C., Garrido, A. (Eds.), Proceedings of the NIR Publications. NIR, Chichester, pp. 67–75.

Drogoudi, P.D., Pantelidis, G., 2011. Effects of position on canopy and harvest time on fruit physico-chemical and antioxidant properties in different apple cultivars. Sci. Hort. 129, 752–760.

ElMasry, G., Wang, N., Vigneault, C., Qiao, J., ElSayed, A., 2008. Early detection of apple bruises on different background colors using hyperspectral imaging. LWT 41, 337–345.

ElMasry, G., Wang, N., Vigneault, C., 2009. Detecting chilling injury in Red Delicious apple using hyperspectral imaging and neural networks. Postharvest Biol. Technol. 52, 1–8.

Ferguson, I., Volz, R., Woolf, A., 1999. Preharvest factors affecting physiological disorders of fruit. Postharvest Biol. Technol. 15, 255–262.

Grimm, E., Khanal, B.P., Winkler, A., Knoche, M., Köpcke, D., 2012. Structural and physiological changes associated with the skin spot disorder in apple. Postharvest Biol. Technol. 64, 111–118.

Hall, M.A., 1998. Correlation-based Feature Subset Selection for Machine Learning. University of Waikato, Hamilton, New Zealand [PhD thesis].

Huang, M., Lu, R., 2010. Apple mealiness detection using hyperspectral scattering technique. Postharvest Biol. Technol. 58, 168–175.

Kavdir, I., Guyer, D.E., 2004. Comparison of artificial neural networks and statistical classifiers in apple sorting using textural features. Biosyst. Eng. 89, 331–344.

Kim, M.S., Chen, Y.R., Mehl, P.M., 2001. Hyperspectral reflectance and fluorescence imaging system for food quality and safety. Trans. ASABE 44, 721–729.
Kleynen, O., Leemans, V., Destain, M.F., 2003. Selection of the most efficient wavelength bands for 'Jonagold' apple sorting. Postharvest Biol. Technol. 30, 221–232.
Lee, K., Kang, S., Delwiche, S.R., Kim, M.S., Noh, S., 2008. Correlation analysis of hyperspectral imagery for multispectral wavelength selection for detection of defects on apples. Sens. Instrumen. Food Qual. 2, 90–96.
Leemans, V., Magein, H., Destain, M.F., 2002. On-line fruit grading according to their external quality using machine vision. Biosyst. Eng. 83, 397–404.
Lleó, L., Roger, J.M., Herrero-Langreo, A., Diezma-Iglesias, B., Barreiro, P., 2011. Comparison of multispectral indexes extracted from hyperspectral images for the assessment of fruit ripening. J. Food Eng. 104, 612–620.
Lu, R., Chen, Y.R., Park, B., 1999. Hyperspectral imaging for detecting bruises in apples. In: ASAE Annual International Meeting, Paper No. 99-3120, 18–21 July, Toronto, Canada.
Lu, R., 2003. Detection of bruises on apples using near-infrared hyperspectral imaging. Trans. ASAE 46, 523–530.
Lu, R., 2004. Multispectral imaging for predicting firmness and soluble solids content of apple fruit. Postharvest Biol. Technol. 31, 147–157.
Lu, R., Peng, Y., 2006. Hyperspectral scattering for assessing peach fruit firmness. Biosyst. Eng. 93, 161–171.
Lu, R., 2007. Nondestructive measurements of firmness and soluble solids content for apple fruit using hyperspectral scattering images. Sensing Instr. Food Qual. Safety 1, 19–27.
Mehl, P.M., Chao, K., Kim, M.S., Chen, Y.R., 2002. Detection of defects on selected apple cultivars using hyperspectral and multispectral image analysis. Appl. Eng. Agric. 18, 219–226.
Mehl, P.M., Chen, Y.R., Kim, M.S., Chan, D.E., 2004. Development of hyperspectral imaging technique for the detection of apple surface defects and contaminations. J. Food Eng. 61, 67–81.
Mendoza, F., Lu, R., Ariana, D., Cen, H., Bailey, B.B., 2011. Integrated spectral and image analysis of hyperspectral scattering data for prediction of apple fruit firmness and soluble solids content. Postharvest Biol. Technol. 62, 149–160.
Nicolai, B., Beullens, K., Bobelyn, E., Peirs, A., Saeys, W., Theron, K.I., Lammertyn, J., 2007. Nondestructive measurements of fruit and vegetable quality by means of NIR spectroscopy: a review. Postharvest Biol. Technol. 46, 99–118.
Peng, Y., Lu, R., 2006. An LCTF-based multispectral imaging system for estimation of apple fruit firmness. Part II. Selection of optimal wavelengths and development of prediction models. Trans. ASAE 49, 269–275.
Peng, Y., Lu, R., 2008. Analysis of spatially resolved hyperspectral scattering images for assessing apple fruit firmness and soluble solids content. Postharvest Biol. Technol. 48, 52–62.
Qin, J., Lu, R., Peng, Y., 2009. Prediction of apple internal quality using spectral absorption and scattering properties. Trans. ASABE 52, 499–507.
Rasband, W.S., 1997–2011. ImageJ. U.S. National Institutes of Health, Bethesda, MD, USA, http://imagej.nih.gov/ij/
Schatzki, T.F., Haff, R.P., Young, R., Can, I., Le, L.C., Toyofuku, N., 1997. Defect detection in apples by means of X-ray imaging. Trans. ASAE 40, 1407–1415.
Shahin, M.A., Tollner, E.W., McClendon, R.W., Arabnia, H.R., 2002. Apple classification based on surface bruises using image processing and neural networks. Trans. ASAE 45, 1619–1627.
Sun, D.W., 2008. Computer Vision Technology for Food Quality Evaluation, 1st ed. Academic Press/Elsevier, San Diego, CA, USA.
Sun, D.W., 2010. Hyperspectral Imaging for Food Quality Analysis and Control, 1st ed. Academic Press/Elsevier, San Diego, CA, USA.
Upchurch, B.L., Throop, J.A., Aneshansley, D.J., 1994. Influence of time, bruise-type, and severity on near-infrared reflectance from apple surfaces for automatic bruise detection. Trans. ASAE 37, 1571–1575.
Wang, J., Nakano, K., Ohashi, S., Kubota, Y., Takizawa, K., Sasaki, Y., 2011. Detection of external insect infestations in jujube fruit using hyperspectral reflectance imaging. Biosyst. Eng. 108, 345–351.
Wen, Z., Tao, Y., 2000. Dual-camera NIR/MIR imaging for stem-end/calyx identification in apple defect sorting. Trans. ASAE 43, 449–452.
Witten, I.H., Frank, E., 2005. Data Mining. Practical Machine Learning Tools and Techniques, 2nd ed. Morgan Kaufmann Publishers/Elsevier, San Francisco, CA, USA.
Xing, J., Bravo, C., Jancso, P., Ramon, H., De Baerdemaeker, J., 2005. Bruise detection on Golden Delicious apples by using hyperspectral imaging with multiple wavebands. Biosyst. Eng. 90, 27–36.
Xing, J., Jancso, P., De Baerdemaeker, J., 2007. Stem-end/calyx identification on apples using contour analysis in multispectral images. Biosyst. Eng. 96, 231–237.